Monthly Notices
of the
ROYAL ASTRONOMICAL SOCIETY
MNRAS **493,** 2463–2471 (2020) doi:10.1093/mnras/staa416

Sky Quality Meter and satellite correlation for night cloud-cover analysis at astronomical sites

S. Cavazzani,[1,2]★ S. Ortolani,[1,2] A. Bertolo,[3] R. Binotto,[3] P. Fiorentin,[4] G. Carraro,[1] I. Saviane[5] and V. Zitelli[6]

[1]*Department of Physics and Astronomy, University of Padova, Vicolo dell'Osservatorio 3, 35122 Padova, Italy*
[2]*INAF–Osservatorio Astronomico di Padova, Vicolo dell'Osservatorio 5, 35122 Padova, Italy*
[3]*Regional Environmental Prevention and Protection Agency of Veneto, Via Ospedale Civile 24, 35121 Padova, Italy*
[4]*Department of Industrial Engineering, University of Padova, Via Gradenigo 6a, 35131 Padova, Italy*
[5]*European Southern Observatory, Alonso de Cordova, 3107 Santiago, Chile*
[6]*INAF–OAS Osservatorio di Astrofisica e Scienza dello Spazio di Bologna, Via Gobetti 93/3, 40129 Bologna, Italy*

Accepted 2020 February 6. Received 2020 February 5; in original form 2019 October 7

ABSTRACT

The analysis of night cloud cover is very important for astronomical observations in real time, considering a typical observation time of about 15 minutes, and to provide statistics. In this article, we use the Sky Quality Meter (SQM) for high-resolution temporal analysis of the La Silla and Asiago (Ekar Observatory) sky: 3 and 5 minutes respectively. We investigate the annual temporal evolution of the natural contributions of the sky at a site not influenced by artificial light at night (ALAN) and at one highly influenced. We also make a correlation between *GOES* and *Aqua* satellite data and ground-based SQM data to confirm the relationship between the SQM data and cloud cover. We develop an algorithm that allows the use of the SQM for night cloud detection and reach correlations with the nighttime cloud cover detected by the *GOES* and *Aqua* satellites of 97.2 per cent at La Silla and 94.6 per cent at Asiago. Our algorithm also classifies photometric (PN) and spectroscopic nights (SN). We measure 59.1 per cent PN and 21.7 per cent SN for a total percentage of clear nights of 80.8 per cent at La Silla in 2018. The respective Ekar Observatory values are 31.1 per cent PN, 24.0 per cent SN and 55.1 per cent of total clear night time. Application to the SQM network would involve the development of long-term statistics and large data forecasting models for site testing and real-time astronomical observation.

Key words: atmospheric effects – instrumentation: detectors – light pollution – site testing.

1 INTRODUCTION

Artificial light at night (ALAN) increases night-sky brightness, creating the greatest visible effect of light pollution and, in particular, influencing astronomical observations at contaminated sites. In the last decades, light pollution has become a global-scale phenomenon (Kyba et al. 2015), as evidenced by the growing interest from scientists in the fields of astronomy (Patat 2008; Puschnig, Posch & Uttenthaler 2014; Zhang et al. 2016), ecology, biology (Holker et al. 2010; Gaston et al. 2013; Manfrin et al. 2017) and medicine (Kloog et al. 2009; Stevens et al. 2013). The study of this strongly interdisciplinary subject has been rapidly increasing, as evidenced by the growing literature on the subject (Mulder et al. 2015). Light pollution is produced by two main components: the natural component, in turn divided into terrestrial and extraterrestrial, and the artificial component caused by human activities (ALAN). We analyse Sky Quality Meter (SQM) data for two sites with a high temporal resolution at La Silla and Asiago (Ekar Observatory) in 2018: 3 and 5 minutes respectively (see Table 1). The SQM is one of the main tools for light pollution analysis. The main features are described in Cinzano (2005, 2007). Other tools are described in Hanel et al. (2017). SQM networks are widely used, as described in Bertolo et al. (2019), Espey & McCauley (2014), Posch, Binder & Puschnig (2018) and Pun & So (2012).

Fig. 1 shows the topographical maps of the two sites with their respective night images (2018 average) captured by the Visible Infrared Imaging Radiometer Suite (VIIRS) sensor on board the joint NASA/NOAA *Suomi National Polar-orbiting Partnership* (*Suomi NPP*) satellite. The choice of sites gives us the comparison between a site influenced by ALAN and one that is not contaminated.

We study the contribution of the main natural factors (e.g. Milky Way, Moon, zodiacal light, etc.) and also show how the cloud cover

★ E-mail: stefano.cavazzani@unipd.it

Table 1. Geographic characteristics of the analysed sites.

Site	Lat.	Long.	Altitude (km)
Asiago (Ekar Observatory)	45°50′	11°34′	1.366
La Silla	−29°15′	−70°43′	2.347

influences the readings of the SQM. One of the pioneers of cloud-contribution studies was Roy Garstang (Garstang 2007).

Garstang's study was developed further and linked to the new SQM networks in Bara' (2016), Bara', Lima & Zamorano (2019) and Ribas et al. (2016). The contribution of clouds and their impact on the biosphere is also studied in Jechow et al. (2017).

In this article, we develop an algorithm based on SQM data for cloud-cover analysis and correlate this result with satellite data. We analysed the VIIRS data to measure the mean magnitude in 2018 in clear-sky conditions to calibrate the model empirically. We calculated the cloud cover at night through the *Geostationary Operational Environmental Satellite* (*GOES*) and the *Aqua* satellite, in particular its Moderate Resolution Imaging Spectro-radiometer (MODIS) tool. The former is a geostationary satellite, while the latter is a polar satellite. Finally, we correlated these results with the SQM data.

The application of our algorithm to the SQM network would collect long- and short-term statistics of sky brightness and cloud cover at night, two fundamental parameters for astronomical observation. We can extrapolate important information for real-time observations and forecast modelling using only the SQM tool.

The layout of the article is as follows: Section 2 illustrates the details of the SQM measurements and ancillary satellite data products; in Section 3 we describe the method used to derive information about cloud cover from the SQM data; in Sections 4 and 5 we correlate our SQM cloud detection algorithm with satellite data for the temporal analysis of photometric and spectroscopic nights at La Silla and Asiago, respectively. In Section 6 we associate uncertainties with the correlations. Finally, in Section 7 we discuss the results and present our conclusions.

2 SQM MEASUREMENTS AND ANCILLARY SATELLITE DATA PRODUCTS

The sky-brightness measurements were carried out at both sites with a Sky Quality Meter–Lens Ethernet (SQM-LE) pointed toward the zenith. The SQM-LE measures the darkness of the night sky to provide readings of magnitudes per square arcsecond (mpsas=mag arcsec^{-2}) through an Ethernet connection. A light sensor provides the microcontroller with a light level, while the the temperature sensor compensates the readings for various operating temperatures. In this analysis we use the ancillary satellite data provided by *GOES*, *Aqua*/MODIS and VIIRS.

The *Aqua* satellite's orbit has a perigee of 691 km and an apogee of 708 km. *Aqua* MODIS views the entire surface of the Earth every 1–2 d, acquiring data in 36 spectral bands or groups of wavelengths. The cloud cover is analysed using bands 20–36 (see Table 2). MODIS band 31 corresponds to the wavelength of *GOES* band 4 (see Table 3). The *GOES* satellite has a geostationary orbit at an altitude of 35 800 km.

We processed the *GOES* data using MCIDAS-V, a free software package (for model details, see Cavazzani et al. 2011; Cavazzani, Ortolani & Zitelli 2015). In this analysis we use a single image per night (02:45 local time). This makes the *GOES* data highly comparable with MODIS data. The MODIS data are analysed through the Giovanni interactive visualization and analysis website.[1] This tool is designed for visualization and analysis of atmosphere daily global 1° × 1° products. There is a single image per night. Finally, the VIIRS data provide the mean annual magnitude in clear-sky conditions to calibrate the threshold. The VIIRS sensor is a *Suomi NPP* satellite tool. The imaging day/night band (DNB) provides global data at 742 m spatial resolution and is a calibrated radiometer. The DNB visible bands have a broad spectral range of 0.5–0.9 μm centred on 0.7 μm and have the ability to collect low-light imagery at night.

3 METHODS AND DATA ANALYSIS

First we used the annual mean light emission detected by VIIRS above the two analysed sites. We used the light-emission value converted into magnitude provided by the Light Pollution Map website.[2] The site refers to the World Atlas of artificial night sky brightness (Falchi et al. 2016) and gives a mean value in clear conditions of 21.9 for La Silla and 20.9 for Ekar Observatory in 2018. We used the derived magnitude to calibrate our algorithm for detecting clouds empirically and to classify whether a site is contaminated by ALAN or not.

We analysed the SQM data for 2018 at La Silla and Asiago (Ekar Observatory). A measurement with high temporal resolution is carried out every 3 and 5 minutes, respectively, from 9:00 pm to 5:00 am local time. We then analysed the data of the *GOES* satellite[3] as described in Cavazzani et al. (2011) and correlated it with *Aqua* satellite data using the method described in Cavazzani et al. (2015) and Cavazzani, Ortolani & Zitelli (2017). We correlated each night's satellite data with SQM data measured from the ground.

At La Silla, we have a triple validation of *GOES–Aqua*–SQM data and at Asiago a dual validation of *Aqua*–SQM, since this site is outside the *GOES* field of view. A first important consideration on which our analysis was based is the detection that, at a site not subject to light pollution such as La Silla, the sky appears darker during covered nights, while it appears brighter at a contaminated site like Asiago. We also note how the trend is made irregular by the presence of clouds in both cases. For this reason, we calculate the standard deviation between three values at La Silla while, in the case of the Ekar Observatory, we calculate the maximum half-dispersion between two values, due to the lower temporal resolution of the instrument. We have chosen intervals of 9 minutes for La Silla and 10 minutes for Asiago to exclude gradual variations due to the presence of the Milky Way or the Moon. Our algorithm reproduces the sky brightness and cloud-cover trends during the night. The standard deviation is higher when the night is covered, whereas in the case of a clear night it is very low.

The conversion of the SQM standard deviation into a cloud-cover fraction is carried out through monthly temporal analysis: time intervals are classified as cloudy when the standard deviation is above the threshold function described in Section 3.1 (e.g. if we analyse about 240 hours per month, then if the standard deviation is above the threshold for 20 of these hours we get $20/240 \times 100 = 8.3$ per cent of cloud-cover fraction).

[1] https://giovanni.gsfc.nasa.gov
[2] https://www.lightpollutionmap.info
[3] https://www.class.noaa.gov

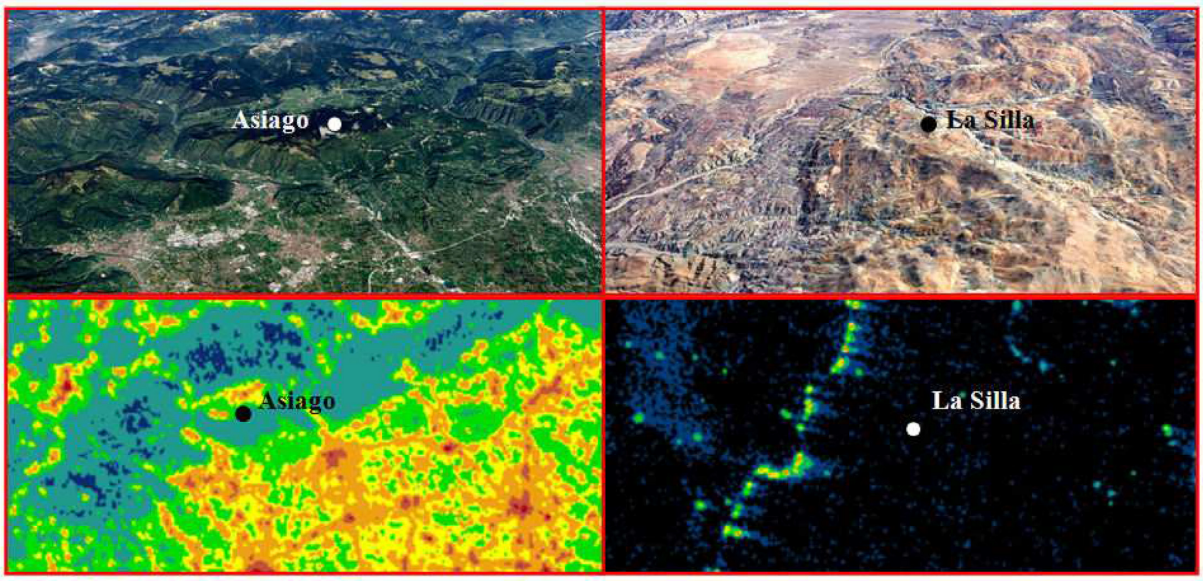

Figure 1. Location of the site analysed. The top left panel shows the topographical characteristics of Asiago, where the point indicates the Ekar Observatory, and the bottom left panel shows the average light emission in 2018 for the Asiago area detected by VIIRS. The panels on the right show the same characteristics for the La Silla observatory.

Table 2. MODIS bands. The spatial resolution of the bands is 1 km.

Primary use	Band	Bandwidth [μm]
Surface/cloud temperature		
	20	3.660–3.840
	21	3.929–3.989
	22	3.929–3.989
	23	4.020–4.080
Atmospheric temperature		
	24	4.433–4.498
	25	4.482–4.549
Cirrus cloud water vapour		
	26	1.360–1.390
	27	6.535–6.895
	28	7.175–7.475
Cloud properties		
	29	8.400–8.700
Ozone		
	30	9.580–9.880
Surface/cloud temperature		
	31	10.780–11.280
	32	11.770–12.270
Cloud-top altitude		
	33	13.185–13.485
	34	13.485–13.785
	35	13.785–14.085
	36	14.085–14.385

Table 3. *GOES* bands and resolution.

	Window	Passband [μm]	Resolution [km]
BAND1	Visible	0.55–0.75	4
BAND2	Microwaves	3.80–4.00	4
BAND3	H_2O	6.50–7.00	4
BAND4	IR	10.20–11.20	4
BAND6	CO_2	13.30	8

Table 4. Variable thresholds as a function of site magnitude.

Magnitude	σ	Magnitude	σ
22.0	0.050	19.5	0.164
21.5	0.073	19.0	0.186
21.0	0.096	18.5	0.209
20.5	0.118	18.0	0.232
20.0	0.141	17.5	0.255

3.1 Photometric and spectroscopic nights classification using the SQM

In this section, we describe the empirical mathematical model used to understand in what circumstances the value of the standard deviation indicates the presence of clouds. The choice of standard deviation threshold is fundamental for night classification. First of all, we have empirically set the threshold as a function of the yearly mean magnitude M (see equation 1) detected by VIIRS (see Fig. 1): 21.9 for La Silla and 20.9 for Ekar Observatory. We assumed a linear relationship between the SQM SD threshold and the M value detected by a satellite, considering that both data families are expressed as magnitudes. This relationship is given by the empirical formula:

$$\sigma = A \cdot M + B. \quad (1)$$

where the values of A and B are obtained empirically through the correlation with *GOES* and *Aqua* satellite data. We assumed a minimum threshold value of 0.050 for a site with a magnitude of 21.9 ($0.050 = 21.9A + B$) and a value of 0.100 for a site with magnitude 20.9 ($0.100 = 20.9A + B$). We calculate the values in Table 4 by solving a linear system and obtaining $A = -0.04545$ and $B = 1.05000$.

Note that the algorithm uses a lower threshold for sites less contaminated by ALAN, in agreement with fig. 8 of Puschnig, Wallner & Posch (2020).

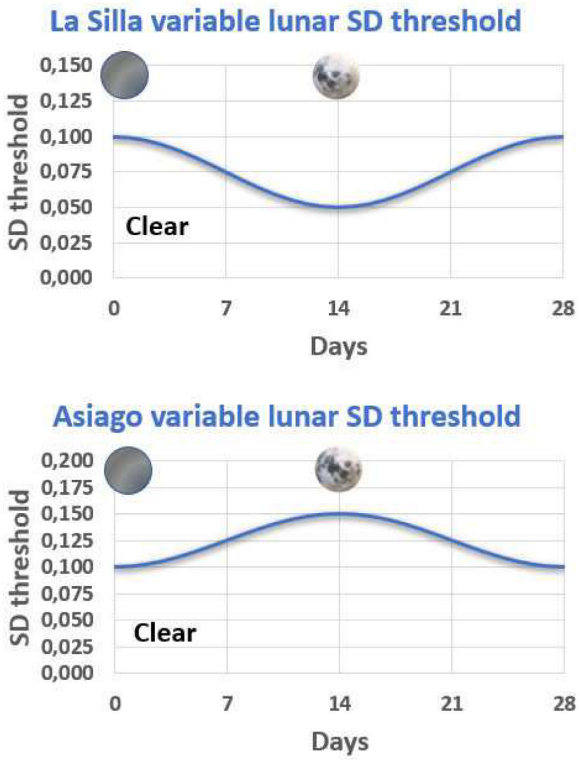

Figure 2. The top panel shows the standard deviation (SD) threshold trend according to the lunar cycle for a site not contaminated by ALAN (La Silla), the bottom panel that for a contaminated site (Asiago). The SD threshold is expressed in mpsas=mag arcsec^{-2} (y-axis). In this case we considered a 28-day moon cycle.

The second factor that influences the threshold is the presence of the Moon, as shown in Fig. 2. We argue that, at a site that is not contaminated by ALAN and close to the new Moon, clouds block the natural contribution of the sky, magnifying the fluctuations detected by the SQM. Therefore our algorithm uses a higher threshold during these days. During nights near the full Moon, clouds are illuminated only from above and therefore they dampen the fluctuations encountered by the SQM, making the sky more homogeneous. The opposite occurs at a site contaminated by ALAN. The clouds are strongly illuminated from below and this, during days without the presence of the Moon, eliminates all fluctuations due to the natural light of the sky, lowering the SQM standard deviation. During nights near the full Moon, clouds are instead illuminated from above and below, increasing the SQM fluctuations. Therefore, we suggest approximating the threshold by the following function for a site not contaminated by ALAN:

$$\sigma(x) = \frac{\Lambda}{2} \cdot \cos\left[\frac{2\pi}{T}(x)\right] + \sigma, \quad (2)$$

where Λ is the minimum threshold value, x the days starting from the new Moon, σ is provided by Table 4 and T is the lunar synodic period chosen for the classification. The function for a contaminated site becomes

$$\sigma(x) = -\frac{\Lambda}{2} \cdot \cos\left[\frac{2\pi}{T}(x)\right] + \sigma.$$

We classify the nights using this function, following the definitions of photometric night (PN) and spectroscopic night (SN). We consider as PN those nights with an interval greater than 6 hours under the threshold function, while SP denotes those with an interval greater than 2 hours. We analyse local time from 9:00 pm to 5:00 am for a total of 4800 monthly data ($N = 160$ per night) at La Silla and 2280 ($N = 96$ per night) at Asiago.

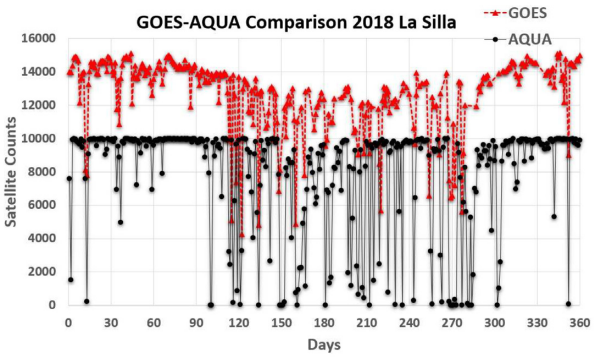

Figure 3. Comparison between *GOES* and MODIS daily data in 2018 at La Silla. The top trend represents the *GOES* data and shows the seasonal temperature: the winter months are the coldest and the most covered. The trend of MODIS is instead normalized to the value of 10 000 satellite units.

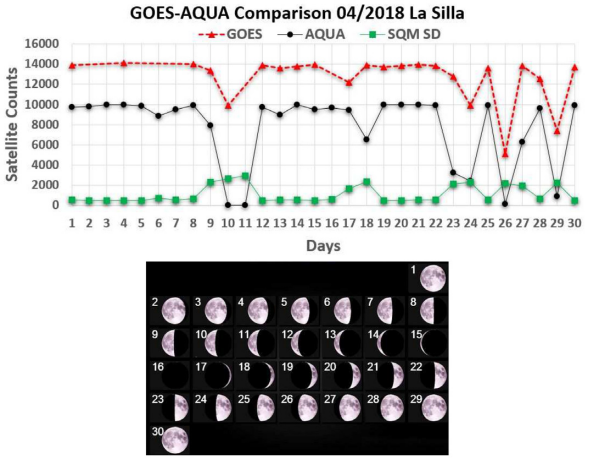

Figure 4. The top panel shows a triple comparison of *GOES*, MODIS and the average standard deviation of SQM data ($SQM_{SD} = \bar{\sigma} \times 10\,000$). Cloudy nights show a drop in satellite unit count and an increase in average stardard deviation. The bottom panel shows the monthly lunar cycle.

4 LA SILLA OBSERVATORY

Fig. 3 shows a comparison between *GOES* and MODIS data in 2018 at La Silla. The cloud cover detected is 81.3 and 80.1 per cent, respectively. The punctual correlation between the two satellite data sets, calculated with the Pearson correlation index, for this site is 96.6 per cent.

Fig. 4 shows in detail the month of 2018 April (top panel) with the respective lunar cycle (bottom panel). Choosing this month allowed us to analyse four basic cases: clear or cloudy sky on nights near the new Moon and clear or cloudy sky near the full Moon. The top trend represents the *GOES* data, the central trend represents the MODIS data and the bottom trend is the average standard deviation of the SQM data every 9 minutes. The MODIS data are analysed as in Cavazzani et al. (2015) for comparison with *GOES* data, while we used the following conversion to compare the mean standard

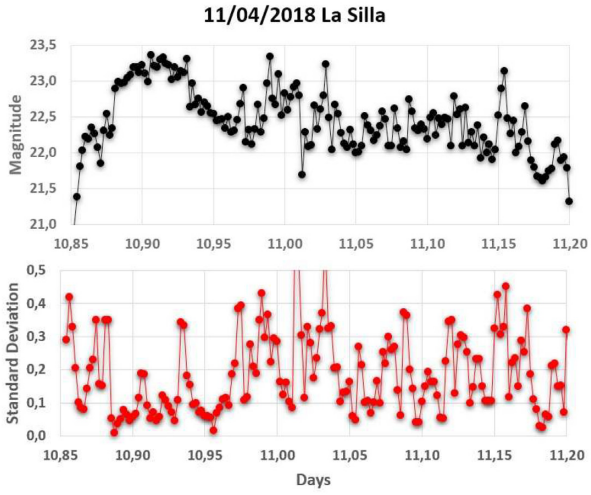

Figure 5. Trend of SQM values on a night with cloudy sky in the last quarter of the Moon at La Silla, 2018 April 10 (top panel) and the respective standard deviation trend every 9 minutes (bottom panel). The SQM values and SD are expressed in mpsas=mag arcsec$-^2$ (y-axis).

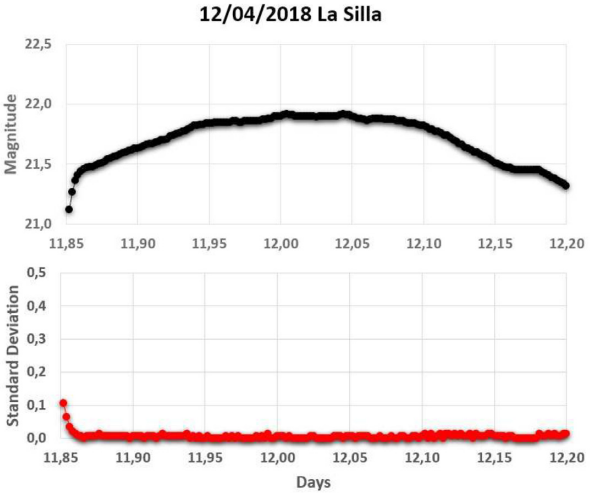

Figure 6. Trend of SQM values on a night with clear sky in the last quarter of the Moon at La Silla, 2018 April 12 (top panel) and the respective standard deviation trend every 9 minutes (bottom panel). The SQM values and SD are expressed in mpsas=mag arcsec^{-2} (y-axis).

deviation with the satellite data:

$$SQM_{\rm SD} = \bar{\sigma} \times 10\,000.$$

We see a low standard deviation in correspondence with clear-sky conditions and vice versa. We analyse in detail the nights with the four conditions described above: Fig. 5 shows the trend of a covered night on the day of the last Moon quarter (top panel). The presence of clouds makes the sky darker at a site not contaminated by ALAN. The magnitude value is greater than 23 and remains about 22 for the whole night, with large fluctuations. The bottom panel shows the respective standard deviations calculated every 9 minutes; the average value is 0.33. Fig. 6 shows the SQM data for a last quarter clear night. During this night, the maximum value is 21.8 while the average standard deviation is 0.03. Fig. 7 shows the status of a covered night near the full Moon. The maximum value is 18.2, while the minimum is 16.0; the average standard deviation is

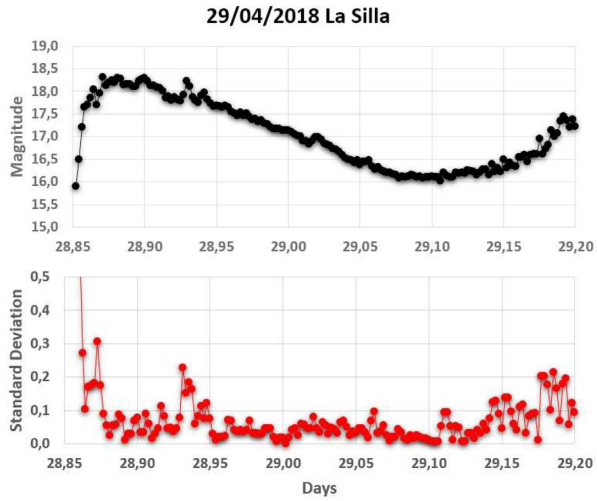

Figure 7. Trend of SQM values on a night with cloudy sky near the full Moon at La Silla, 2018 April 28 (top panel) and the respective standard deviation trend every 9 minutes (bottom panel). The SQM values and SD are expressed in mpsas=mag arcsec^{-2} (y-axis).

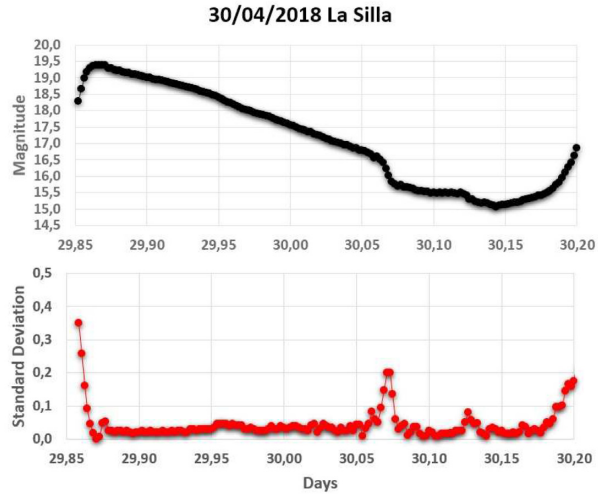

Figure 8. Trend of SQM values on a night with clear sky near the full Moon at La Silla, 2018 April 29 (top panel) and the respective standard deviation trend every 9 minutes (bottom panel). The SQM values and SD are expressed in mpsas=mag arcsec^{-2} (y-axis).

0.18. Finally, Fig. 8 shows the trend of a full Moon clear night: the maximum value is 19.4, while the minimum is 15.0. The average standard deviation is 0.05. By comparison of Figs 7 and 8, we see that, at a site without ALAN in the presence of the Moon, clouds make the sky brighter in the first part of the night and darker in the central part.

Table 5 shows the results obtained in terms of clear-sky time. This type of analysis provides the sum of photometric and spectroscopic observation times at a site with very stable night-time conditions: in particular, a night that begins with a clear sky remains good (Cavazzani, Ortolani & Zitelli 2012). Column 2 shows the clear-sky percentage detected by *Aqua*, column 3 that detected by *GOES* (see Section 2) and column 4 that from the standard deviation of SQM data. Column 5 shows the daily correlation between the two satellites (A–G) and column 6 that between *GOES* and the SQM standard deviation (G–SQM). The last line gives the annual

Table 5. Night clear-sky percentage at La Silla in 2018. Triple daily correlation between *GOES* and *Aqua* (A–G) satellites and the SQM algorithm for night cloud detection (G–SQM). Column 2 shows the clear-sky percentage detected by *Aqua*, column 3 that detected by *GOES* and column 4 that from the standard deviation of SQM data. Column 5 shows the daily correlation between the two satellites (A–G), column 6 that between *GOES* and the SQM standard deviation (G–SQM). The last line gives the annual average values.

La Silla	*GOES–Aqua*–SQM correlations				
2018	*Aqua*	*GOES*	SQM	A–G	G–SQM
1	90.9	91.3	–	99.2	–
2	93.3	92.8	91.8	99.0	97.5
3	92.2	91.3	90.2	98.2	97.3
4	77.9	78.4	78.6	99.0	99.5
5	70.9	71.3	71.4	99.2	99.8
6	60.9	61.3	61.5	99.2	99.5
7	64.1	68.6	72.4	91.0	90.5
8	75.2	75.3	74.8	99.8	98.8
9	72.7	78.3	79.4	88.8	97.3
10	76.8	82.1	85.0	89.4	92.8
11	94.2	92.9	91.9	97.4	97.5
12	92.6	91.8	91.4	98.4	99.0
Mean	80.1	81.3	80.8	96.6	97.2

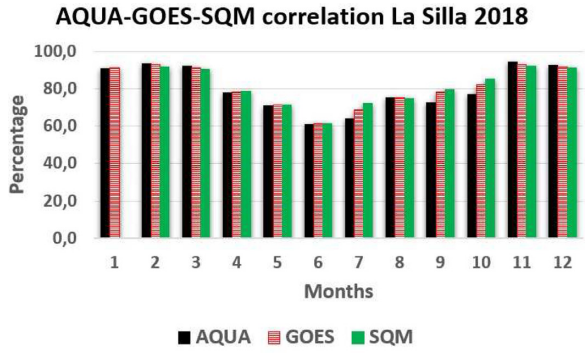

Figure 9. Comparison of the clear-sky percentages (*y*-axis) measured with *Aqua*, *GOES* and the SQM standard deviation in 2018 at La Silla.

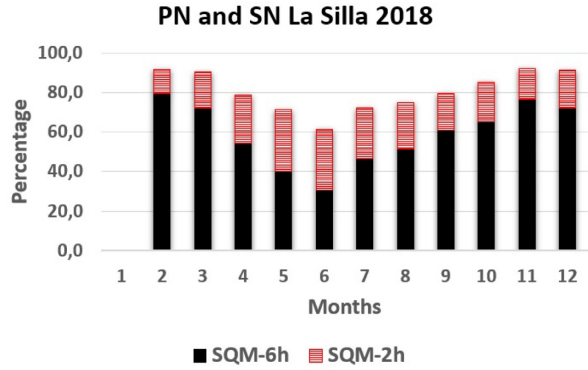

Figure 10. Photometric and spectroscopic nights calculated by the SQM algorithm for cloud detection in 2018 at La Silla.

average values. A comparison between the results provided by *GOES*, *Aqua* and our algorithm is shown in Fig. 9. Fig. 10 and Table 6 show the percentages of PN and SP at La Silla in 2018 calculated with the SQM standard deviation. We carried out a further

Table 6. Night clear-sky percentage at la Silla in 2018. Percentage of photomentric (SQM-6h) and spectroscopic (SQM-2h) nights.

2018	SQM-6h	SQM-2h	SQM
1	–	–	–
2	79.4	12.4	91.8
3	72.1	18.1	90.2
4	54.3	24.3	78.6
5	40.1	31.3	71.4
6	30.7	30.8	61.5
7	46.6	25.8	72.4
8	51.4	23.4	74.8
9	61.1	18.3	79.4
10	65.2	19.8	85.0
11	76.6	15.3	91.9
12	72.1	19.3	91.4
Mean	59.1	21.7	80.8

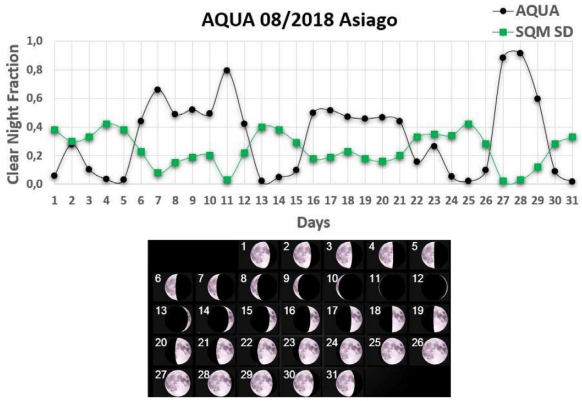

Figure 11. The top panel shows a comparison between MODIS and the average maximum half-dispersion of SQM data ($SQM_{SD} = \bar{\sigma} \times 10\,000$). Cloudy nights show a drop in satellite unit count and an increase in average maximum half-dispersion. The bottom panel below shows the monthly lunar cycle.

check using a sample: one month of ground data.[4] We have chosen the month of May for its climatic complexity, in order to verify the algorithm in various climatic conditions. We measure a PN percentage of 38.7 per cent and a SN percentage of 29.0 per cent from the ground data with a SQM punctual correlation on a single night of 96.3 per cent.

5 EKAR OBSERVATORY IN ASIAGO

We perfomed the same analysis for Ekar Observatory in Asiago. Fig. 11 shows the correlation between the mean maximum half-dispersion and the *Aqua* data at Asiago in 2018 August. We analyse in detail the four main conditions that can be found on a site. The top panel of Fig. 12 shows a clear night with a new Moon with its relative maximum half-dispersion (bottom panel). The night reaches magnitude values greater than 21. The top panel of Fig. 13 shows a first quarter Moon night with clouds. This shows that, at a contaminated site, clouds decrease the magnitude of the sky. The bottom panel shows the SQM maximum half-dispersion. We can see an example of a spectroscopic night in its first part. The

[4] http://archive.eso.org/cms/eso-data/ambient-conditions.html

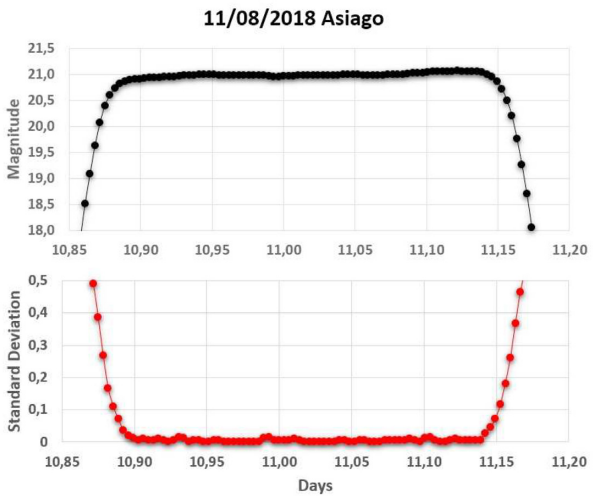

Figure 12. Trend of SQM values on a night with new Moon and clear sky at Ekar Observatory, 2018 August 10 (top panel) and the respective maximum half-dispersion trend every 10 minutes (bottom panel). The SQM values and maximum half-dispersion are expressed in mpsas=mag arcsec^{-2} (y-axis).

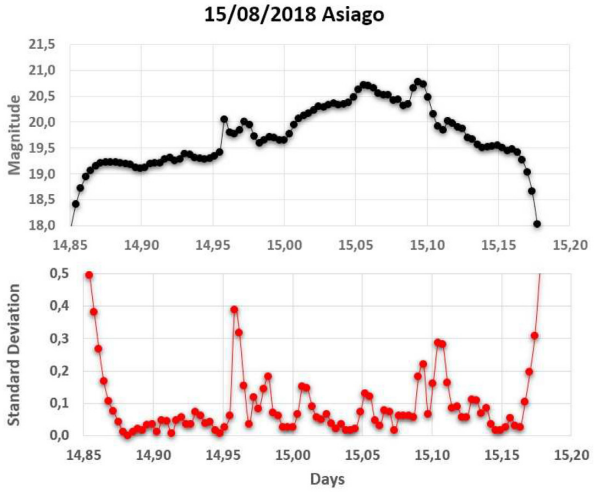

Figure 13. Trend of SQM values on a night with first Moon quarter, cloudy sky at Ekar Observatory, 2018 August 15 (top panel) and the respective maximum half-dispersion trend every 10 minutes (bottom panel). The SQM values and maximum half-dispersion are expressed in mpsas=mag arcsec^{-2} (y-axis).

top panel of Fig. 14 shows a full Moon covered night. The lower panel shows how the presence of clouds illuminated from above and below increases the SQM maximum half-dispersion. This explains the use of the variable lunar threshold shown in Fig. 2. Finally, Fig. 15 shows a clear night next to the full Moon with its respective maximum half-dispersion. Asiago is a site highly contaminated by ALAN (see Fig. 1) and also has high cloud-cover conditions, around 40 per cent per year.[5] It does not have stable night-time conditions, therefore the low temporal and spatial resolution of the *Aqua* satellite does not provide results in terms of observation time, but rather in terms of photometric nights. The algorithm classifies intervals longer than 6 hours as photometric nights and intervals longer than 2 hours as spectroscopic nights.

[5]http://www.oapd.inaf.it

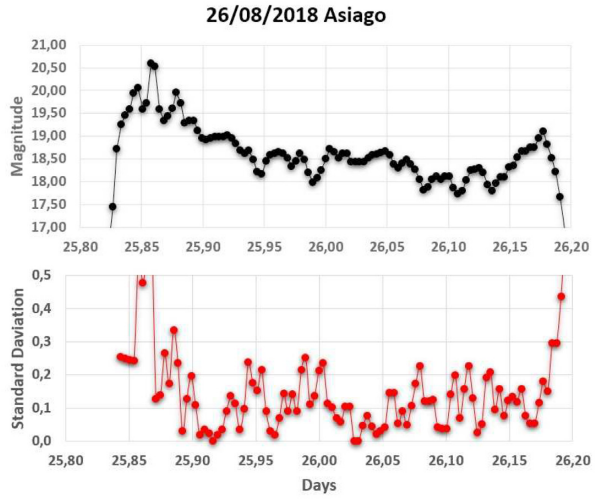

Figure 14. Trend of SQM values on a night with full Moon, cloudy sky at Ekar Observatory, 2018 August 26 (top panel) and the respective maximum half-dispersion trend every 10 minutes (bottom panel). The SQM values and maximum half-dispersion are expressed in mpsas=mag arcsec^{-2} (y-axis).

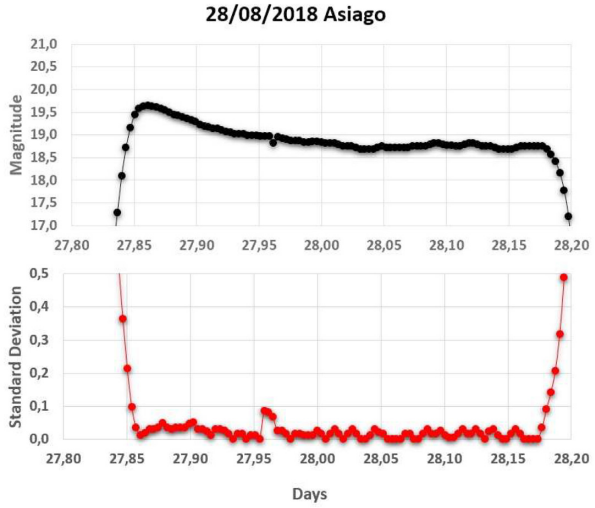

Figure 15. Trend of SQM values on a night with almost full Moon, clear sky at Ekar Observatory, 2018 August 28 (top panel) and the respective maximum half-dispersion trend every 10 minutes (bottom panel). The SQM values and maximum half-dispersion are expressed in mpsas=mag arcsec^{-2} (y-axis).

Table 7 shows the results obtained: column 2 gives the *Aqua* satellite values and column 3 the values of photometric nights detected by the SQM. Column 4 shows the monthly point correlation between the two groups of data (S-SQM-6h). Column 5 shows the percentage added by spectroscopic nights. The sum of columns 4 and 5 gives the annual percentage of site use. The last line gives the annual average values. Fig. 16 shows the comparison between the photometric nights detected by satellite and those calculated by our algorithm. Fig. 17 shows the sum of the monthly averages of the photometric and spectroscopic nights. We carried out the same further check with a sample month of ground data[6] made at La Silla. We have chosen the month of September for its climatic complexity, in order to verify the algorithm in various climatic

[6]http://www.oapd.inaf.it

Table 7. Night clear sky at Asiago in 2018. Daily correlation between *Aqua* satellite and the SQM algorithm for night cloud detection (column 4, S-SQM-6h). The table shows the clear-sky percentage: columns 2 and 3 show the percentages of photometric nights, while column 5 gives the percentage of spectroscopic observation time of at least a 2-hour interval.

Asiago	*Aqua*–SQM correlations			
2018	*Aqua*	SQM-6h	S-SQM-6h	SQM-2h
1	30.1	32.5	91.6	23.2
2	24.2	25.9	94.1	27.3
3	23.9	25.1	95.8	22.6
4	–	–	–	–
5	25.2	24.1	96.2	20.5
6	24.3	26.5	92.3	24.1
7	31.2	30.2	96.5	27.6
8	35.4	35.8	98.6	28.5
9	42.0	38.5	87.8	19.8
10	36.7	37.3	97.9	24.9
11	26.7	28.1	95.1	18.2
12	36.4	37.9	94.8	27.3
Mean	30.6	31.1	94.6	24.0

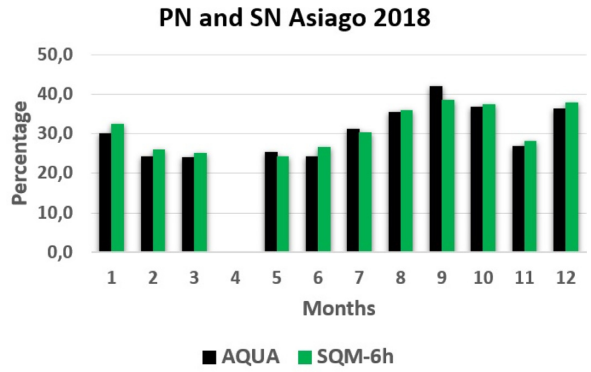

Figure 16. Comparison of the clear-sky percentages (*y*-axis) measured with *Aqua* and the SQM maximum half-dispersion in 2018 at Ekar Observatory.

Figure 17. Photometric and spectroscopic nights calculated by the SQM algorithm for cloud detection in 2018 at Ekar Observatory.

conditions. We measure a PN percentage of 36.7 per cent and a SN percentage of 20.0 per cent from the ground data, with a SQM punctual correlation on a single night of 94.1 per cent. In some cases, we found a discrepancy between the ground time used and the SQM data, due to high humidity with clear-sky conditions. We performed a further analysis at Asiago due to the instability of the site. We calculated the usable time in the first (20:00–01:00) and second part (01:00–06:00) of the night. This can be useful for sites with a high percentage of cloud cover, to understand the part of the night that is better statistically for observations.

Table 8. Night clear sky at Asiago in 2018 obtained through the SQM maximum half-dispersion. Column 2 gives the percentage of spectroscopic observation time of at least 2-hour intervals in the first part of the night (20:00–01:00), column 3 that in the second part of the night (01:00–06:00).

Month	SQM-2h (20:00–01:00)	SQM-2h (01:00–06:00)
January	52	55
February	53	55
March	45	53
April	46	56
May	47	50
June	57	60
July	65	69
August	63	68
September	58	60
October	53	58
November	47	52
December	53	57
Mean	53	58

Table 8 shows the results of this analysis: the second part of the night is statistically better at Asiago, with the highest discrepancy during the spring, in conjunction with the melting of snow.

6 CORRELATION UNCERTAINTY BETWEEN THE SQM AND SATELLITE DATA

We associated two types of uncertainties with our correlation measurement: a monthly statistical uncertainty and a punctual nightly uncertainty. Table 5 shows the monthly night clear-sky percentages obtained by satellite and the SQM readings at La Silla. We consider the monthly statistical uncertainty between the two satellites as given by the absolute value of the difference between columns 2 and 3, while that between *GOES* and SQM is given by the absolute value of the difference between columns 3 and 4. The annual averages are $\epsilon_{\mathrm{A-G}} = 0.2$ per cent and $\epsilon_{\mathrm{G-SQM}} = 0.5$ per cent, respectively, at La Silla in 2018. The punctual uncertainty, as in Cavazzani et al. (2015), provides the nightly correspondence between the satellite analysis and the SQM data analysis and is given by the complementary corellation coefficient in column 6. The annual average is $\epsilon^{\mathrm{Nightly}}_{\mathrm{G-SQM}} = 2.8$ per cent (e.g. if we associate an error of 1 night relative to 1 month, this means that an error of 1 night corresponds to about 3 per cent).

The same analysis is carried out for Asiago observing in Table 7. We calculate the monthly statistical uncertainty through the absolute value of the difference between columns 2 and 3, and the punctual uncertainty with the complementary corellation coefficient in column 4. The annual averages are $\epsilon_{\mathrm{A-SQM}} = 0.5$ per cent and $\epsilon^{\mathrm{Nightly}}_{\mathrm{A-SQM}} = 5.4$ per cent, respectively, at Ekar Observatory in 2018.

Finally, we estimated the total uncertainty through the uncertainty propagation, also considering the discrepancies between our algorithm and the ground data in the presence of particular climatic conditions (e.g. high humidity). We considered the ground data of a complex climatic condition month for each site, as described in Sections 4 and 5. The punctual uncertainty between the ground data and SQM data is $\epsilon_{\mathrm{La\,Silla}} = 3.7$ per cent at La Silla and $\epsilon_{\mathrm{Asiago}} = 5.9$ per cent at Asiago. The total nightly uncertainty

can be estimated through the formulae

$$\epsilon_{\rm Total} = \sqrt{(\epsilon^{\rm Nightly}_{\rm G-SQM})^2 + (\epsilon_{\rm La\,Silla})^2}$$

and

$$\epsilon_{\rm Total} = \sqrt{(\epsilon^{\rm Nightly}_{\rm A-SQM})^2 + (\epsilon_{\rm Asiago})^2},$$

yielding an uncertainty of about 5.0 per cent at La Silla and 8.0 per cent at Asiago. In a future work, we will deepen the correlation between the ground data and our algorithm for further validation and improvements.

7 DISCUSSION AND CONCLUSION

The analysis of night-time cloud cover is still an open problem. Satellites are designed primarily for daily analysis and have some limitations during the night. In this article, we describe a new algorithm for the nocturnal analysis of cloud cover making use of SQM data. We verified the results through correlation with polar and geostationary satellite data and a sample of ground data for the most significant periods, namely the most climatically variable months.

Tables 5 and 7 show the results of this correlation. This allows the use of a single instrument for measuring two factors that are important for astronomical observations: sky brightness and and average cloud cover at night. The installation of the SQM instrument associated with the algorithm described will provide the extraction of objective and low-cost statistics of night cloud cover. This would be implemented in all current short- and long-term forecasting models. It has also been shown that the presence of clouds has opposite effects at sites affected and unaffected by light pollution. We also showed how the Moon also has an opposite effect for the two conditions analysed. Cloud cover with a full Moon reduces the sky brightness from magnitude 15.0 to 16.0 and lowers the SD at La Silla. With a full Moon, clouds induce smaller variations than with a new Moon at an uncontaminated site. Clouds also filter moonlight, so the sky becomes darker. At Asiago, the magnitude changes from 18.5 to 18.0 and the maximum half-dispersion rises. In addition to astronomical applications, this study also explains ALAN effects in all conditions, with their consequences on flora and fauna.

Our algorithm shows how the SQM could be used to detect night-sky brightness and nocturnal cloud cover simultaneously. The empirical calibration of the threshold is a function of the magnitude detected by VIIRS (see Table 4) and of the lunar cycle (see Fig. 2). We observed SQM reading changes during intervals of 9 minutes for La Silla and 10 minutes for Asiago to exclude gradual variations due to the presence of the Milky Way or the Moon. These intervals are also in agreement with typical astronomical observation times.

The choice of 6-hour and 2-hour intervals also classifies photometric and spectroscopic nights (see Tables 6 and 7). The high temporal resolution of the SQM allows real-time observation of night clouds, improving the quality and calibration of astronomical observations. The high correlation between the satellite and our algorithm, as described in Section 6, also extrapolates the seasonal trends of the two sites (see Figs 10 and 17).

In conclusion, we described a new algorithm for studying sky brightness and cloud cover during the night using only the SQM tool. This simple and cheap tool was extremely sensitive for night cloud detection and very useful for collecting large data archives. This procedure can be applied to the entire SQM network, contributing to the development and improvement of astronomical telescope scheduling.

ACKNOWLEDGEMENTS

This activity is supported by the INAF (Istituto Nazionale di Astrofisica) funds allocated to the Premiale ADONI MIUR. Most of the *GOES* data used in this article are from the Comprehensive Large Array-data Stewardship System (CLASS), which is an electronic library of NOAA environmental data. This website provides capabilities for finding and obtaining data, particularly NOAA *Geostationary Operational Environmental Satellite* data. MODIS data were provided by the Giovanni – Interactive Visualization and Analysis website. We also refer to the 3D atmospheric reconstruction project at Prato Piazza (Italy). We thank Astronomer Researcher Marina Orio for her careful reading and advice to increase the clarity of this article. We acknowledge funding from the Italian Ministry of Education, University and Research (MIUR) through the Dipartimenti di eccellenza project 'Science of the Universe'. Finally, we thank the University of Padua for support for this search (Research grant, type A, Rep. 138, Prot. 3022, 26/10/2018).

REFERENCES

Bara' S., 2016, R. Soc. Open Sci., 3, 160541
Bara' S., Lima R. C., Zamorano J., 2019, Sustainability, 11, 3070
Bertolo A., Binotto R., Ortolani S., Sapienza S., 2019, J. Imaging, 5, 56
Cavazzani S., Ortolani S., Zitelli V., Maruccia Y., 2011, MNRAS, 411, 1271
Cavazzani S., Ortolani S., Zitelli V., 2012, MNRAS, 419, 3081
Cavazzani S., Ortolani S., Zitelli V., 2015, MNRAS, 452, 2185
Cavazzani S., Ortolani S., Zitelli V., 2017, MNRAS, 471, 2616
Cinzano P., 2005, ISTIL Intern. Rep., 9, v. 1.4, Available at: http://www.inquinamentoluminoso.it/download/sqmreport.pdf
Cinzano P., 2007, ISTIL Internal Report, Available at: http://unihedron.com/projects/sqm-l/sqmreport2.pdf
Espey B., McCauley J., 2014, Light. Res. Technol., 46, 67
Falchi F. et al., 2016, Science Advances, 2, 1600377
Garstang R. H., 2007, The Observatory, 127, 1
Gaston K., Bennie J., Davies T. W., Hopkins J., 2013, Biol. Rev., 88, 912
Hanel A. et al., 2017, J. Quant. Spectrosc. Radiat. Transfer, 205, 278
Holker F., Wolter C., Perkin E., Tockner K., 2010, Trends in Ecology and Evolution, 25, 681
Jechow A., Kollth Z., Ribas S. J., Spoelstra H., Hlker F., Kyba C. C. M., 2017, Scientific Reports, 7, 6741
Kloog I., Haim A., Stevens R. G., Portnov B. A., 2009, Chronobiology International, 26, 108
Kyba C. et al., 2015, Scientific Reports, 5, 8409
Manfrin A. et al., 2017, Front. Environ. Sci , Available at: https://www.frontiersin.org/articles/10.3389/fenvs.2017.00061/full
Mulder C. et al., 2015, Advances in Ecological Research, 53, 1
Patat F., 2008, A&A, 481, 575
Posch T., Binder F., Puschnig J., 2018, J. Quant. Spectrosc. Radiat. Transfer, 211, 144
Pun C. S. J., So C. W., 2012, Environ. Monit. Assess., 184, 2537
Puschnig J., Posch T., Uttenthaler S., 2014, J. Quant. Spectrosc. Radiat. Transfer, 139, 64
Puschnig J., Wallner S., Posch T., 2020, MNRAS, 492, 2622
Ribas S. J., Torra J., Figueras F., Paricio S., Canal-Domingo R., 2016, Int. J. Sustainable Lighting, 35, 32
Stevens R. G., Brainard G. C., Blask D. E., Lockley S. W., Motta M. E., 2013, AJPM, 45, 343
Zhang J., Fan Z., Yan J. Z., Kumar Y. B., Li H. B., Gao D. Y., Jiang X. J., 2016, PASP, 128, 1

This paper has been typeset from a TEX/LATEX file prepared by the author.